HHS Public Access

Author manuscript

Mol Cancer Ther. Author manuscript; available in PMC 2020 May 01.

Published in final edited form as:

Mol Cancer Ther. 2019 May ; 18(5): 937–946. doi:10.1158/1535-7163.MCT-18-0862.

Vemurafenib Inhibits Active PTK6 in *PTEN-null* Prostate Tumor Cells

Darren J. Wozniak[1], **Ben Hitchinson**[1], **Milica Gilic**[1], **Wenjun Bie**[1], **Vadim Gaponenko**[1,2], **Angela L. Tyner**[1,2,*]

[1]Department of Biochemistry and Molecular Genetics, University of Illinois at Chicago, Chicago, IL

[2]University of Illinois Cancer Center, University of Illinois at Chicago, Chicago, IL

Abstract

Protein tyrosine kinase 6 (PTK6, also called BRK) is overexpressed and activated in human prostate cancer. Loss of the tumor suppressor PTEN, a frequent event in prostate cancer, leads to PTK6 activation at the plasma membrane and its oncogenic signaling. The small molecule inhibitor vemurafenib, also known as PLX4032, and its tool analog PLX4720 were designed to inhibit constitutively active BRAF V600E, yet they also have potent effects against PTK6. Vemurafenib is used in the treatment of metastatic melanoma but its efficacy in prostate cancer has not been assessed. When activated at the plasma membrane, PTK6 promotes signaling through FAK, EGFR, and ERK1/2, and we show this can be blocked by vemurafenib. In addition, PTK6-mediated cell growth, migration, and invasion are inhibited upon vemurafenib administration. Using a flank xenograft model, vemurafenib treatment reduced tumor burden. Using saturation transfer difference NMR and molecular docking, we demonstrate that vemurafenib binds in the active site of PTK6 inhibiting its activation. These structural studies provide insight into the PTK6-vemurafenib complex which can be utilized for further refinement chemistry while functional studies demonstrate that active PTK6 is a viable drug target in prostate cancer.

INTRODUCTION

Prostate cancer has surpassed lung cancer as the most common cancer, and it is the second leading cause of cancer-related death among American men. In 2019, an estimated 174,650 men will be diagnosed with prostate cancer, and 31,620 men will die of the disease in the United States alone (1). With early detection at a local or regional stage and proper treatment, the 5-year survival for prostate cancer approaches 100%. A portion of prostate cancers that reach stage IV with metastases to the lymph nodes, bone, and other organs have a much worse outcome with 5-year survival at 30% and are referred to as metastatic castration-resistant prostate cancer (1). These types of cancers are resistant to androgen ablation therapy and are not well controlled with traditional chemotherapy. The need to

*Corresponding author: University of Illinois Cancer Center, Department of Biochemistry and Molecular Genetics, M/C 669, 900 South Ashland Avenue, Chicago, Illinois 60607, Phone: 312-996-7964, atyner@uic.edu.

Disclosure of Potential Conflicts of Interest: The authors have no conflicts of interest to report.

This is an original manuscript; data have not been published elsewhere.

develop new drugs that inhibit the metastatic potential and prime the cell death response of prostate cancer cells is evident.

The intracellular Protein Tyrosine Kinase 6 (PTK6, also called BRK) is activated at the plasma membrane in human prostate cancer (2–4) where it phosphorylates tyrosine residues on the scaffolding protein BCAR1, leading to enhanced cell migration (2). PTK6 also promotes tyrosine phosphorylation of FAK, both at the activation site (Y576/577) and at the GRB2 binding site (Y925) (3). Though not essential, PTK6-mediated activation of FAK promotes survival signaling and protects cells from anoikis (5). PTK6 directly phosphorylates AKT on tyrosine residues 315 and 326 and promotes its activation by EGF in prostate cells (6). Survival signaling induced by PTK6 is dependent on AKT, suggesting that AKT is a critical player downstream of PTK6 (3). PTK6 also phosphorylates EGFR at Y845, stimulating its activity and inhibiting its turnover (7). Through these pathways, PTK6 regulates cell migration as well as the growth and viability of prostate cancer cells.

Increased levels of PTK6 expression are detected in metastatic human prostate cancer and correlate with reduced survival (2,5). PTK6 contributes to the aggressive, metastatic profile of the *PTEN* null PC3 prostate cancer cell lines. Stable knockdown of PTK6 impaired cell proliferation and colony formation of PC3 cells (8) while siRNA mediated knockdown of PTK6 decreased cell migration and invasion (5). Knockdown of PTK6, but not SRC, rendered cells unable to escape anoikis under suspended growth conditions suggesting that PTK6 is a key player in protecting cancer cells from apoptosis due to anchorage independence (3). PC3 cells with knockdown of PTK6 did not survive to give rise to tumors when injected into the tail veins of mice, while PC3 cells with control scrambled siRNA formed metastatic tumors (5). These data support roles for PTK6 in cancer metastasis.

Genetic or epigenetic loss of the tumor suppressor PTEN commonly occurs in late-stage prostate cancer and correlates with cancer-specific mortality (9). Loss of PTEN yields unrestricted PI3K/AKT signaling, yet targeting this pathway alone has not been efficacious (10) suggesting that other oncogenes are activated upon PTEN deletion beyond the PI3K/AKT axis. Increased activation of PTK6 at the plasma membrane has been detected in mouse and human prostate cancer cells and tissues lacking functional PTEN (5,11). Membrane-associated active PTK6 promotes epithelial to mesenchymal transition (5). Recently, we demonstrated that PTK6 is a substrate of the protein phosphatase activity of PTEN, and PTEN specifically targets activating phosphorylation of PTK6 (11). Loss of PTEN leads to increased activation of PTK6. Disruption of the mouse *Ptk6* gene led to reduced tumorigenesis following conditional disruption of *Pten* in the mouse prostate, supporting a role for PTK6 in prostate cancer *in vivo*. These data suggest that targeting active PTK6 in PTEN-deficient prostate cancer may be beneficial.

Tyrosine kinase inhibitors have been used in the treatment of several types of cancer including prostate cancer (12). To date, no kinase inhibitors that specifically target PTK6 are used in the clinic. The small molecule inhibitor vemurafenib (PLX4032) was developed against the mutated form of the serine/threonine kinase BRAF, BRAFV600E. Surprisingly, vemurafenib displays activity against a range of kinases, but is potent at inhibiting mutant BRAF and PTK6 (13,14). Here, we provide insight into how vemurafenib binds and inhibits

PTK6 in the PTEN-deficient PC3 cell line *in vitro* and *in vivo*, reducing prostate tumor growth. These data strongly suggest that combination therapies incorporating PTK6 inhibitors are promising and warrant future investigation.

MATERIALS AND METHODS

Immortalized human cell lines.

The prostate cancer cell line PC3 (CRL-1435), human breast cancer cell lines MDA-MB-231 (HTB-26), MDA-MB-468 (HTB-132) and T47D (HTB-133) and pancreatic cancer cell line MIA PaCa-2 (CRL-1420) were obtained from ATCC (Manassas, VA). PC3 cells were cultured in F-12K Medium (Mediatech, Inc., Manassas, VA) supplemented with 10% FBS (Atlanta Biologicals, Flowery Branch, GA). MDA-MB-231 and T47D cell lines were cultured in RPMI 1640 Medium (GE Healthcare Life Sciences, Logan, UT) supplemented with 10% FBS. MIA PaCa-2 cells were cultured in DMEM Medium (GE Healthcare Life Sciences, Logan, UT) supplemented with 10% FBS. MDA-MB-468 cell line was cultured in MEM Medium (Mediatech, Inc) supplemented with 10% FBS and 1x MEM non-essential amino acids (GIBCO Life technologies). The Phoenix Ampho viral packaging cell line was cultured in DMEM (Hyclone Laboratories, Inc., Logan, Utah) supplemented with 10% FBS. Fresh media with DMSO (control vehicle) or vemurafenib was applied to cells one hour prior to harvesting for total cell lysates for immunoblotting. All cell lines are regularly tested for mycoplasma contamination using the MycoAlert Mycoplasma Detection Kit according to the manufacturer's instructions (Lonza Group Ltd., Basel, Switzerland). pBABE-puro vectors were used to generate PC3 Vector and PC3 Palm-PTK6-YF stable pools of cell lines that were selected in media containing 2 μg/ml puromycin as previously described (6). Total cell lysates were prepared and subjected to immunoblotting as previously described (6).

RNA silencing.

The small inhibitor duplex RNA (siRNA) targeting human BRAF (15) was synthesized by Dharmacon (Lafayette, CO). The sequence of sense strand was as follows: 5'-AGAAUUGGAUCUGGAUCAUdTdT-3'. The Universal Negative Control siRNA #1 (Sigma, St. Louis, MO) was used as a control. For siRNA transfection, PC3 Vector and PC3 Palm-PTK6-YF were grown in F-12K Medium (Mediatech, Inc., Manassas, VA) supplemented with 10% FBS (Atlanta Biologicals, Flowery Branch, GA) and 2 μg/ml puromycin. The day before transfection, $1X10^5$ cells/well were plated in 6 well plates (Corning, MA) with F-12K Medium supplemented with 10% FBS and without antibiotics. 160 nM siRNA and 10 μl Lipofectamine RNAiMAX from Invitrogen (Grand Island, NY) were used for transfection per well when cells were 70 – 80% confluent. Culture media was changed at 24 hours after transfection and 15 minutes prior to harvesting at 72 hours post transfection.

Antibodies.

Anti-human PTK6 (G6), anti-Raf-B (F-7) and anti-FAK (C-20) were purchased from Santa Cruz Biotechnology (Dallas, TX). Anti-EGFR and anti-P-PTK6 (Tyr-342) were purchased from Millipore (Temecula, CA). Anti-Ki67 was purchased from Abcam (Cambridge, MA). Antibodies directed against AKT, P-AKT (Thr-308), P-AKT (Ser-473), P-BCAR1

(Tyr-165), cleaved Caspase-3, P-EGFR (Tyr-845), P-FAK (Tyr-397), P-FAK (Tyr-576/577), p44/42 MAPK, p44/42 MAPK (Thr202/Tyr204) and P-FAK (Tyr-925) were purchased from Cell Signaling Technology (Danvers, MA). Anti-BCAR1 antibody was purchased from BD Biosciences (San Jose, CA). Antibodies directed against β-actin (AC-15) were purchased from Sigma-Aldrich (St. Louis, MO). Donkey anti-rabbit or sheep anti-mouse antibodies conjugated to horseradish peroxidase were used as secondary antibodies (GE Healthcare, Pittsburgh, PA) and detected by chemiluminescence with SuperSignal West Dura substrate from Thermo Fisher Scientific (Rockford, IL).

Proliferation, scratch migration, and transwell invasion assays.

Prior to all cell culture experiments, cells were dissociated from plastic culture dishes with Trypsin-EDTA (Mediatech, Inc., Manassas, VA) and live cells were quantified by trypan blue exclusion followed by counting using the Countess Automated Cell Counter (Invitrogen, Carlsbad, CA). For proliferation assays, 1×10^5 cells were seeded in triplicate into 6-well plates on day 0. Two cell lines, PC3 Vector and PC Palm-PTK6-YF were treated with either DMSO or 1 μM vemurafenib (PLX4032, Selleckchem, Houston, TX). Drug and vehicle were added to the cells on day 1. Each following day, cells in 3 wells were trypsinized and resuspended in culture media and quantified. Live cells were quantified by trypan blue exclusion followed by counting using the Countess Automated Cell Counter (Invitrogen, Carlsbad, CA). For scratch migration assays, 5×10^5 were plated into 6-well plates and allowed to grow to confluence. Cells were then serum starved in culture media containing 0.1% FBS for 24 hours. After serum starving, a scratch was made in the confluent cells with a 200 μL pipette tip. Then, growth media containing 20% serum with DMSO or 1 μM PLX4032 was added back to the cells. Pictures of wound closure were taken 24 and 48 hours after the scratch. For transwell invasion assays, Matrigel (Corning Inc., Corning, NY) was diluted to 1 mg/ml in serum-free media and 25 μl was pipetted onto the 24-well transwell membrane (Corning Inc., Corning, NY) and allowed to set. 1×10^5 cells were then placed in the upper chamber with growth media in both chambers. The following day, cells in the upper and lower chambers were serum starved with media containing 0.1% FBS. After 24 hours, the media in the upper chamber was changed to contain either 0.1% FBS with DMSO or 1 μM vemurafenib in DMSO, while the media in the lower chamber contained 20% FBS as a chemoattractant with DMSO or 1 μM vemurafenib in DMSO. After 24 hours, cells remaining in the upper chamber were removed with a cotton swap and cells that had invaded were stained with crystal violet and quantified.

Xenograft assay.

Animal studies were conducted in accordance with the animal protocol approved by the UIC Institutional Animal Care and Use Committee. Male athymic nude CrTac:NCr-*Foxn1*^{nu} sp/sp mice were purchased from Taconic (Rensselaer, NY). 2×10^6 cells resuspended in 100 μl of 1:1 Matrigel (Corning Inc., Corning, NY): PBS were injected subcutaneously into the flanks of 7 week old mice. Each animal received an injection into both the left and right flanks. Four groups of animals were used, with three animals in each group. The groups were as follows: (i) mice injected with PC3 Vector cells and fed a normal chow diet; (ii) mice injected with PC3 Vector cells fed chow containing 417mg/kg PLX4720 (Plexxikon Inc., Berkeley, CA); (iii) mice injected with PC3 Palm-PTK6-YF cells and fed a normal

chow diet; and (iv) mice injected with PC3 Palm-PTK6-YF cells fed chow containing 417mg/kg PLX4720. Modified diet was started once palpable tumors were observed. Tumors were measured every other day until animals reached a humane endpoint.

Immunostaining.

Cells cultured on 8-well chamber slides (Thermo Fisher Scientific) and treated with vehicle or 1 μM Vemurafenib for 24 hours were fixed using Carnoy's solution (ethanol-chloroform-acetic acid, 6:3:1). For immunofluorescence, anti-PTK6 PY342 and anti-cleaved caspase 3 were detected using biotinylated goat anti-rabbit and streptavidin-conjugated Alexa Fluor 488 purchased from Invitrogen (Carlsbad, CA). Counterstaining of cells and tissues for immunofluorescence was performed with 4',6-diamidino-2-phenylindole (DAPI). Xenograft tumors were collected from mice, formalin-fixed and paraffin-embedded. Tissues were subjected to immunostaining as described in (5). For immunohistochemistry Ki67 was detected using horseradish peroxidase-conjugated goat anti-rabbit antibodies in the presence of 3,3'-diaminobenzidine (DAB).

Quantification and Statistics.

Immunoblot quantification was done with ImageJ (16). For all experiments, at least 3 independent trials were performed. Results are shown as the mean ± standard error of the mean (SEM). For analysis of immunoblot intensities and gene expression, P-values were determined using a two-tailed, unpaired Student's t test (GraphPad Prism 6) and observed variation within groups and across was similar. To quantify fluorescence, Alexa Fluor 488 signals were measured in 15 cells from 3 different images per cell line per treatment and quantified with ImageJ (16). Single cells were selected and pixel intensity was quantified and corrected for background pixel intensity. Calculated fluorescence intensities were normalized to average intensity of DMSO treated cells and expressed as percentages. Results were expressed as averages ± SEM. Students two-tailed *t*-test (GraphPad Prism 7) was used to determine P-values. For mouse studies, no animals were excluded from scoring. Quantitative results from tumor tissue antibody staining were expressed as an average ± SEM, and two-way ANOVA was used to determine P-values. A difference was considered statistically significant if the P-value was less than 0.05. The authors declare that all data are available within the manuscript or supplementary files, or available from the authors upon request.

GST-Fusion protein expression.

GST-tagged mouse PTK6 fusion proteins (Full-length, SH3, SH2, SH3-SH2) were cloned into pGEX-KG, while the GST-PTK6-Catalytic domain was cloned into pGEX2T. Proteins were prepared and purified as described previously (17). Samples were dialyzed into PBS overnight (assay buffer) at 4 °C and subjected to SDS-PAGE to analyze purity.

Nuclear Magnetic Resonance.

^{1}H and Saturation transfer difference (STD) experiments were performed on a Bruker 800 MHz Avance spectrometer equipped with a cryogenic probe. For STD, saturation was achieved with a train of 50 ms Gaussian-shaped pulses applied at field strength of 100 Hz in

the methyl region at −1 ppm. The duration of the saturation pulse was 1 s. Vemurafenib was dissolved in $DMSO_{d6}$ and used at a final concentration of 1 mM. Where relevant, experiments were performed with 10 μM PTK6 fusion proteins in assay buffer containing 10% D_2O and 20% $DMSO_{d6}$. All experiments were carried out at room temperature.

Molecular Docking Simulations.

PLX4032 was docked into the kinase domain of PTK6 using AutoDock Vina (18). The structure of PLX4032 was constructed using the ChemOffice software suite (PerkinElmer, Waltham MA) and energy minimization performed using the MM2 feature. The crystal structure of the PTK6 catalytic domain (5DA3) (19) was used for docking. Grid maps were generated with a 0.375 Å spacing using a grid box of 44–100–44 Å. At least 27 models were generated and assessed for goodness of fit based on STD experiments.

RESULTS

PC3 cells that lack PTEN express a pool of endogenous active PTK6 at the plasma membrane that promotes oncogenic signaling, but much of the PTK6 protein is cytoplasmic and not active (2). Targeted ectopic expression of PTK6 with a mutation of its inhibitory tyrosine residue 447 to phenylalanine (YF) to the plasma membrane by addition of an amino terminal palmitoylation/myristoylation consensus sequence (Palm, Palm-PTK6-YF) greatly increases the active pool of PTK6 (2,20). Active PTK6 is detected by examining phosphorylation of tyrosine residue 342 in the catalytic domain (PY342) using phospho-specific antibodies. Vemurafenib (PLX4032) and its tool analog PLX4720 have been shown to inhibit PTK6 at submicromolar concentrations (13,14,21). To validate these findings, we exposed PC3 cells selected for maintenance of empty vector or overexpression of Palm-PTK6-YF to increasing concentrations of vemurafenib for different times. At a concentration of 100 nM, no effect on ectopic active PTK6 is observed (Fig. 1A). However, when the concentration is increased to 1 μM, substantial inhibition of PTK6 is observed as quickly as 30 minutes. In patients treated with vemurafenib, a steady state human serum concentration of 100 μM (50 μg/ml) has been reported (22). When the compound is incubated with cells for 6 hours, a near complete loss of PTK6 activation is observed (Fig. 1A). Activating phosphorylation of FAK at Y576/577 is regulated by PTK6 (3) and reduced by vemurafenib. Phosphorylation of BCAR1, another PTK6 substrate (2), is also transiently reduced in the presence of vemurafenib. These data suggest that vemurafenib blocks PTK6 activation and downstream signaling.

To confirm reproducibility, experiments were performed in triplicate with vemurafenib using 1 μM treatment for 1 hour on vector control or stable Palm-PTK6-YF expressing PC3 cells (Fig. 1B). Compared with PC3 Vector cells, overexpression of Palm-PTK6-YF promotes activation of FAK (PY576/577) and phosphorylation of the FAK GRB2 binding site (PY925). In addition, Palm-PTK6-YF leads to increased stabilization and activation of EGFR through phosphorylation of EGFR Y845 as previously reported (7). PTK6 has been shown to promote AKT activation (6), and increased activation of AKT (PT308 and PS473) is detected in Palm-PTK6-YF cells. Activation of ERK1/2 (PT202/Y204) was detected in control cells expressing Palm-PTK6-YF, which is likely the result of increased upstream

signaling promoted by PTK6 phosphorylation of FAK at Y925 (23,24) and EGFR at Y845 (7). In the presence of vemurafenib, PTK6-regulated signaling is diminished (Fig. 1B). These data demonstrate that PTK6-mediated phosphorylation of FAK, EGFR, and AKT, and ERK1/2 can be chemically inhibited by vemurafenib in PC3 cells. Relative levels of active PTK6 and downstream phospho-proteins normalized to total protein following treatment with 1 μM vemurafenib for one hour is shown in Figure 1B, lower panel.

To determine if vemurafenib could be acting through inhibition of BRAF in PC3 cells, BRAF expression was knocked down by transient transfection using a well validated siRNA (BRAFsi) (15) (25) and cells were harvested at 72 hours, with transfection of a scrambled siRNA used as a control (SCRsi). Unlike vemurafenib treatment, knockdown of BRAF did not have an effect on PTK6 activity or tyrosine phosphorylation of direct substrates of PTK6 including FAK and EGFR (Fig. 1C), supporting our finding that vemurafenib inhibits PTK6 activity. We detected decreased phosphorylation of ERK1/2, at 72 hours post transfection of BRAF siRNA, because ERK1/2 is downstream of BRAF (Figure 1C).

To further validate the effect of vemurafenib on PTK6 activation and signaling, PC3 cells were subjected to knockdown of endogenous PTK6 by shRNA with two targeting vectors (sh49 and sh52). sh49 targets the 3'UTR and sh52 targets the 5' end of the PTK6 coding sequence. Although levels of active PTK6 and its downstream targets are enhanced in cells overexpressing Palm-PTK6-YF (compare vector and Palm-PTK6-YF lanes in Fig. 1B), activation of endogenous PTK6 is detectable in PC3 cells by immunoblotting with longer exposure (Fig. 1D, shSCR DMSO control). However, upon PTK6 knockdown, the effect of vemurafenib treatment on substrates of PTK6 is attenuated (Fig. 1D), suggesting that effects due to vemurafenib treatment can be attributed to the inhibition of PTK6. A similar decrease in PTK6 signaling is detected following PTK6 knockdown (DMSO, shRNA49 and shRNA52) or treatment with vemurafenib (vemurafenib, shSCR). ERK1/2 activation is not detected in PC3 cells without ectopic expression of active membrane-targeted PTK6 (Fig. 1D).

We examined the ability of vemurafenib to inhibit PTK6 activation at the plasma membrane in cell lines of different origins, including breast (MDA-MB-468, T47D, and MDA-MB-231) and pancreatic cancer (MIA PaCa-2) (Fig. 2). PC3 and MDA-MB-468 cells both lack wild type PTEN and display more striking activation of PTK6 at the plasma membrane. Overexpression of membrane targeted active PTK6 leads to clustering of PTK6 and its substrates in peripheral adhesion complexes (2). In all cell lines, treatment with vemurafenib led to a reduction in PTK6 activation at the membrane compared with vehicle (DMSO) alone (Fig. 2).

Our previous data showed that knockdown of PTK6 by siRNA inhibits the oncogenic properties of PC3 prostate cancer cells (3,5). We aimed to determine if chemical inhibition of PTK6 by vemurafenib would mimic the effects of PTK6 knockdown by siRNA. When Palm-PTK6-YF is overexpressed in PC3 cells, increased growth, migration, and invasion are observed (Fig. 3 A–C). In the presence of 1 μM vemurafenib, PTK6-mediated growth, migration, and invasion are significantly reduced (Fig. 3A–C). Vemurafenib also inhibited

PC3 Vector cell migration and invasion, suggesting that inhibition of endogenous PTK6 also has a critical effect on the invasive phenotype (Fig. 3B and C).

Since our *in vitro* studies show that PTK6 activity and oncogenic potential can be chemically inhibited, we investigated whether this translates into a therapeutic benefit *in vivo.* PC3 cells expressing empty vector or Palm-PTK6-YF were injected into flanks of nude mice as human-in-mouse xenografts. Once palpable tumors were observed (~100 mm^3), each group was fed either normal chow or chow containing 417 mg/kg PLX4720, the tool analog of vemurafenib that has superior bioavailability in mice (26). Tumor volumes were measured once per week and all mice were sacrificed, once one tumor/mouse reached a humane endpoint (41 days post-injection). Although the PC3 Vector cells formed tumors, those expressing Palm-PTK6-YF showed a growth advantage (Fig. 4A, green vs. blue line). The Palm-PTK6-YF-induced growth advantage is significantly reduced when mice are fed the PLX4720 diet (Fig. 4A, green vs. red line). PLX4720 also inhibits endogenous PTK6 *in vivo* and results in reduced growth (Fig. 4A, blue vs. black line). Additionally, tumors harvested from mice fed the PLX4720 diet showed reduced masses in both PC3 Vector and Palm-PTK6-YF cell lines (Fig. 4B and D). At the end of the study, mice in the normal chow group began to lose body weight either due to cachexia or water loss, while mice treated with PLX4720 appeared protected from this body weight loss (Fig. 4C).

Xenograft tumors were formalin fixed and stained for Ki67 and cleaved caspase 3 to determine the impact of vemurafenib on proliferation and apoptosis, respectively. PLX4720 treatment led to a reduction in the number of Ki67 positive proliferating cells (Fig. 4E) and an increase in apoptosis detected by cleaved caspase 3 (Fig. 4F). Thus, vemurafenib is able to inhibit both prostate xenograft tumor growth and survival *in vivo.*

To investigate the direct interaction of vemurafenib with PTK6, we performed saturation transfer difference (STD) nuclear magnetic resonance (NMR) experiments with purified recombinant GST-tagged full length (FL) PTK6, or its SH3, SH2, SH3-SH2, and kinase domains (Fig. 5A) in the absence or presence of the drug. STD signals arise when a small molecule binds a high molecular weight protein. The signals corresponding to the parts of the small molecule directly interacting with the protein have the highest intensities in STD spectra. Initial experiments using 1 mM vemurafenib suggested that the compound aggregated and generated a weak STD signal without the protein (Fig. 5B). The STD spectrum of vemurafenib added to FL PTK6 exhibited signals at 1, 2.7, and 3.8 ppm, corresponding to the methyl and methylene groups of the compound (Fig. 5B). The same signals were also observed in the STD spectrum of vemurafenib with the kinase domain of PTK6 (Fig. 5C), with an additional signal at 2 ppm, suggesting that the main binding site for the drug is located in this region of the protein. The 2.7 ppm methylene signal of vemurafenib was visible in the spectra of GST-tagged SH2 and SH3 domains of PTK6 (Fig. 5C) but also in the presence of GST, suggesting some non-specific binding of the drug to the GST-tag. In contrast to the binding mode of PLX4720 to V600E BRAF revealed by X-ray crystallography (21), no STD transfer was observed for the aromatic portion or the amino groups of the compound, although these signals were visible in the 1D ^1H spectrum of drug (Fig. 5B, inset). This suggests that vemurafenib binds PTK6 differently from BRAF, chiefly employing the propyl tail that is attached to the sulfonamide moiety. This portion was

initially designed to optimally interact with the backbone amide of alanine 594 of BRAF V600E, while fitting into the interior pocket of the mutant kinase (27). Additionally, the azaindole scaffold that is decorated with two phenyl rings is critical for anchoring the drug in the hinge region of the kinase domain of BRAF but is not detected in our STD experiments. To further investigate the relative contributions of the different groups of vemurafenib to binding PTK6, we performed molecular docking of the drug into the crystal structure of its kinase domain (19) (Fig. 5D). In agreement with the STD results, the docking shows direct interaction of the propyl and sulfonamide groups with the kinase, while the rest of the drug points away from the domain.

DISCUSSION

Prostate cancer is the most common malignancy in American men (1). Loss of the tumor suppressor PTEN commonly occurs in late-stage prostate cancer and yields unrestricted PI3K-AKT signaling (9), but targeting this pathway alone has not been effective (10). Identifying novel targets that contribute to the progression of prostate cancer is critical for the development of more effective therapeutics. Here we report that PTK6 activation in human prostate cancer cells with loss of PTEN can be inhibited by vemurafenib. These data suggest a possible off-target therapeutic role for vemurafenib in prostate cancers with active PTK6, and that identification of other PTK6 inhibitors may have utility in the treatment of prostate cancer.

Vemurafenib has been instrumental for treatment of malignant melanoma. In their manuscript describing the discovery of PLX4720, the structurally related vemurafenib precursor compound, Tsai and colleagues biochemically determined the IC50s for PLX4720 against a panel of kinases and reported that PLX4720 inhibits PTK6 similarly to wild type BRAF, with an IC50 of 130 nM (13). In contrast, other kinases, such as the PTK6 family member FRK and the related kinase SRC, required a 10-fold increase in PLX4720 for inhibition, with IC50s of 1,300 nM and 1,700 nM, respectively. In a later study, Vin *et al.* (14) identified additional targets of vemurafenib/PLX4720 using quantitative competitive binding assays and calculated IC50s for vemurafenib/PLX4720 for BRAF V600E and PTK6 that were comparable at 64.78/32.0 for BRAF V600E and 68.0/30.38 nM for PTK6. These findings led us to test the ability of vemurafenib and PLX4720 to inhibit activated PTK6 signaling in prostate cancer cells *in vitro* and *in vivo*. It has been the paradigm that vemurafenib specifically inhibits growth of tumors with the BRAF V600E mutation. While the ERK pathway is inhibited in cells with mutant BRAF V600E, vemurafenib activates ERK signaling in cells with wild type BRAF, through binding and promoting activation of RAF/RAF protein dimers (28,29). PC3 cells have mutant PTEN and p53 but wild type BRAF. In our study, we did not observe enhanced ERK1/2 activation following treatment with 1 μM vemurafenib, and Palm-PTK6-YF induced activation of ERK1/2 was inhibited (Fig. 1B), suggesting specificity for PTK6 over WT-BRAF. In fact, knockdown of WT-BRAF did not have an impact on PTK6 activation and phosphorylation of its substrates (Fig. 1C). Furthermore, addition of vemurafenib to cells with PTK6 knockdown did not significantly reduce activation of downstream targets more than PTK6 knockdown alone, indicating that vemurafenib is acting through PTK6 and not other targets (Fig. 1D).

PTK6 plays roles in promoting growth and survival of several solid tumor types, including prostate and breast tumor cells (4,30), and we demonstrate that vemurafenib-mediated inhibition of PTK6 occurs in multiple cells types, including breast and pancreatic cancer cell lines (Fig. 2). We show vemurafenib-mediated inhibition of PTK6 has an impact on cell growth, migration, and invasion of PC3 cells expressing either endogenous PTK6 (Vector) or ectopic membrane targeted active PTK6 (Palm PTK6-YF) *in vitro* (Fig. 3). Moreover, xenograft tumors generated by the control Vector and Palm PTK6-YF PC3 expressing cells displayed decreased proliferation and increased apoptosis following treatment with the vemurafenib analog PLX4720 (Fig. 4).

Using STD NMR, we demonstrated direct binding of vemurafenib to recombinant GST-PTK6. Experiments with GST-tagged SH3, SH2, SH2-SH3 and kinase domains of PTK6 (Fig. 5A) showed that the drug specifically interacts with the kinase domain of the protein (Fig. 5C). The interaction between vemurafenib and PTK6 relies primarily on the sulfonamide and propyl groups of the drug with minimal involvement from the azaindole portion. The sulfonamide and propyl groups were shown to mediate the specificity of PLX4720 for oncogenic BRAF by preferentially binding the active “DFG-in” conformation of the mutant kinase (13). This was also shown to be the case for vemurafenib binding to BRAF V600E (21). Since the conformation of the DFG region is a crucial determinant of kinase activation (31) and important for vemurafenib binding, we chose to dock the drug into the crystal structure of PTK6 that adopted the active, “DFG-in” conformation (19). Docking suggests that vemurafenib binds at the ATP binding site of the PTK6, with the sulfonamide group of the drug oriented into the active site (Fig. 5D). This orientation places the sulfonamide and propyl groups of the drug within bonding distance of two amino acids in the PTK6 catalytic triad, Lys 219 and Asp 330. Asp 330 also forms part of the PTK6 DFG motif (Fig. 5D). This highly conserved amino acid is vital for vemurafenib binding to a range of kinases (21,32) and is likely important for vemurafenib binding to PTK6. Additionally, docking suggests that the azaindole portion of vemurafenib may interact with the hinge region of the PTK6 kinase domain in a manner similar to binding of the drug to BRAF and ZAK (21,32). However, binding of this portion to PTK6 was not observed in our STD experiments and requires further investigation.

Inhibition of SRC-family kinases by dasatinib has shown some promise in treating the oncogenic phenotype *in vitro* and in murine models (33,34), but its effectiveness in human prostate cancer has been somewhat disappointing, where it did not display a benefit when combined with docetaxel (35). Studies with the BCR-ABL tyrosine kinase inhibitor nilotinib suggested cancer cells gain resistance through up-regulation of ERK (36). Here, we demonstrate that vemurafenib inhibits PTK6-induced signaling pathways including ERK1/2 activation. Specific targeting of PTK6 with vemurafenib alone or in combination therapies in prostate or breast cancers where active PTK6 is detected, including cancers with loss of PTEN, could prove therapeutically beneficial.

ACKNOWLEDGEMENTS

These studies were supported by NIH grant R01CA188427 (ALT, VG). We thank Plexxikon Inc. for providing the PLX4720 for the xenograft experiments, and members of the Tyner and Gaponenko labs for helpful discussion of the work.

REFERENCES

1. ACS. Cancer Facts & Figures 2019. Atlanta: American Cancer Society; 2019.
2. Zheng Y, Asara JM, Tyner AL. Protein-tyrosine Kinase 6 Promotes Peripheral Adhesion Complex Formation and Cell Migration by Phosphorylating p130 CRK-associated Substrate. The Journal of Biological Chemistry 2012;287(1):148–58. [PubMed: 22084245]
3. Zheng Y, Gierut J, Wang Z, Miao J, Asara JM, Tyner AL. Protein tyrosine kinase 6 protects cells from anoikis by directly phosphorylating focal adhesion kinase and activating AKT. Oncogene 2013;32(36):4304–12. [PubMed: 23027128]
4. Zheng Y, Tyner AL. Context-specific protein tyrosine kinase 6 (PTK6) signalling in prostate cancer. Eur J Clin Invest 2013;43(4):397–404. [PubMed: 23398121]
5. Zheng Y, Wang Z, Bie W, Brauer PM, Perez White BE, Li J, et al. PTK6 activation at the membrane regulates epithelial-mesenchymal transition in prostate cancer. Cancer Research 2013;73(17):5426–37. [PubMed: 23856248]
6. Zheng Y, Peng M, Wang Z, Asara JM, Tyner AL. Protein tyrosine kinase 6 directly phosphorylates AKT and promotes AKT activation in response to epidermal growth factor. Molecular and Cellular Biology 2010;30(17):4280–92. [PubMed: 20606012]
7. Li X, Lu Y, Liang K, Hsu JM, Albarracin C, Mills GB, et al. Brk/PTK6 sustains activated EGFR signaling through inhibiting EGFR degradation and transactivating EGFR. Oncogene 2012;31(40): 4372–83. [PubMed: 22231447]
8. Brauer PM, Zheng Y, Wang L, Tyner AL. Cytoplasmic retention of protein tyrosine kinase 6 promotes growth of prostate tumor cells. Cell Cycle 2010;9(20):4190–9. [PubMed: 20953141]
9. Jamaspishvili T, Berman DM, Ross AE, Scher HI, De Marzo AM, Squire JA, et al. Clinical implications of PTEN loss in prostate cancer. Nat Rev Urol 2018;15(4):222–34. [PubMed: 29460925]
10. Markman B, Tao JJ, Scaltriti M. PI3K pathway inhibitors: better not left alone. Curr Pharm Des 2013;19(5):895–906. [PubMed: 22973958]
11. Wozniak DJ, Kajdacsy-Balla A, Macias V, Ball-Kell S, Zenner ML, Bie W, et al. PTEN is a protein phosphatase that targets active PTK6 and inhibits PTK6 oncogenic signaling in prostate cancer. Nat Commun 2017;8(1):1508 doi 10.1038/s41467-017-01574-5. [PubMed: 29142193]
12. Ojemuyiwa MA, Madan RA, Dahut WL. Tyrosine kinase inhibitors in the treatment of prostate cancer: taking the next step in clinical development. Expert Opin Emerg Drugs 2014;19(4):459–70. [PubMed: 25345821]
13. Tsai J, Lee JT, Wang W, Zhang J, Cho H, Mamo S, et al. Discovery of a selective inhibitor of oncogenic B-Raf kinase with potent antimelanoma activity. Proceedings of the National Academy of Sciences of the United States of America 2008;105(8):3041–6. [PubMed: 18287029]
14. Vin H, Ojeda SS, Ching G, Leung ML, Chitsazzadeh V, Dwyer DW, et al. BRAF inhibitors suppress apoptosis through off-target inhibition of JNK signaling. Elife 2013;2:e00969 doi 10.7554/eLife.00969. [PubMed: 24192036]
15. Hingorani SR, Jacobetz MA, Robertson GP, Herlyn M, Tuveson DA. Suppression of BRAF(V599E) in human melanoma abrogates transformation. Cancer Res 2003;63(17):5198–202. [PubMed: 14500344]
16. Schneider CA, Rasband WS, Eliceiri KW NIH Image to ImageJ: 25 years of image analysis. Nature Methods 2012;9, 671–675. [PubMed: 22930834]
17. Vasioukhin V, Tyner AL. A role for the epithelial-cell-specific tyrosine kinase Sik during keratinocyte differentiation. Proc Natl Acad Sci U S A 1997;94(26):14477–82. [PubMed: 9405638]
18. Trott O, Olson AJ. AutoDock Vina: improving the speed and accuracy of docking with a new scoring function, efficient optimization, and multithreading. J Comput Chem 2010;31(2):455–61. [PubMed: 19499576]
19. Thakur MK, Birudukota S, Swaminathan S, Battula SK, Vadivelu S, Tyagi R, et al. Co-crystal structures of PTK6: With Dasatinib at 2.24 A, with novel imidazo[1,2-a]pyrazin-8-amine derivative inhibitor at 1.70 A resolution. Biochem Biophys Res Commun 2017;482(4):1289–95. [PubMed: 27993680]

20. Palka-Hamblin HL, Gierut JJ, Bie W, Brauer PM, Zheng Y, Asara JM, et al. Identification of beta-catenin as a target of the intracellular tyrosine kinase PTK6. J Cell Sci 2010;123(Pt 2):236–45. [PubMed: 20026641]
21. Bollag G, Hirth P, Tsai J, Zhang J, Ibrahim PN, Cho H, et al. Clinical efficacy of a RAF inhibitor needs broad target blockade in BRAF-mutant melanoma. Nature 2010;467(7315):596–9. [PubMed: 20823850]
22. da Rocha Dias S, Salmonson T, van Zwieten-Boot B, Jonsson B, Marchetti S, Schellens JH, et al. The European Medicines Agency review of vemurafenib (Zelboraf(R)) for the treatment of adult patients with BRAF V600 mutation-positive unresectable or metastatic melanoma: summary of the scientific assessment of the Committee for Medicinal Products for Human Use. Eur J Cancer 2013;49(7):1654–61. [PubMed: 23481513]
23. Schlaepfer DD, Hanks SK, Hunter T, van der Geer P. Integrin-mediated signal transduction linked to Ras pathway by GRB2 binding to focal adhesion kinase. Nature 1994;372(6508):786–91. [PubMed: 7997267]
24. Schlaepfer DD, Jones KC, Hunter T. Multiple Grb2-mediated integrin-stimulated signaling pathways to ERK2/mitogen-activated protein kinase: summation of both c-Src- and focal adhesion kinase-initiated tyrosine phosphorylation events. Mol Cell Biol 1998;18(5):2571–85. [PubMed: 9566877]
25. Salvatore G, De Falco V, Salerno P, Nappi TC, Pepe S, Troncone G, et al. BRAF is a therapeutic target in aggressive thyroid carcinoma. Clin Cancer Res 2006;12(5):1623–9. [PubMed: 16533790]
26. Su F, Viros A, Milagre C, Trunzer K, Bollag G, Spleiss O, et al. RAS mutations in cutaneous squamous-cell carcinomas in patients treated with BRAF inhibitors. N Engl J Med 2012;366(3): 207–15. [PubMed: 22256804]
27. Bollag G, Tsai J, Zhang J, Zhang C, Ibrahim P, Nolop K, et al. Vemurafenib: the first drug approved for BRAF-mutant cancer. Nat Rev Drug Discov 2012;11(11):873–86. [PubMed: 23060265]
28. Poulikakos PI, Zhang C, Bollag G, Shokat KM, Rosen N. RAF inhibitors transactivate RAF dimers and ERK signalling in cells with wild-type BRAF. Nature 2010;464(7287):427–30. [PubMed: 20179705]
29. Hatzivassiliou G, Song K, Yen I, Brandhuber BJ, Anderson DJ, Alvarado R, et al. RAF inhibitors prime wild-type RAF to activate the MAPK pathway and enhance growth. Nature 2010;464(7287): 431–5. [PubMed: 20130576]
30. Goel RK, Lukong KE. Tracing the footprints of the breast cancer oncogene BRK - Past till present. Biochim Biophys Acta 2015;1856(1):39–54. [PubMed: 25999240]
31. Treiber DK, Shah NP. Ins and outs of kinase DFG motifs. Chem Biol 2013;20(6):745–6. [PubMed: 23790484]
32. Mathea S, Abdul Azeez KR, Salah E, Tallant C, Wolfreys F, Konietzny R, et al. Structure of the Human Protein Kinase ZAK in Complex with Vemurafenib. ACS Chem Biol 2016;11(6):1595–602. [PubMed: 26999302]
33. Nam S, Kim D, Cheng JQ, Zhang S, Lee JH, Buettner R, et al. Action of the Src family kinase inhibitor, dasatinib (BMS-354825), on human prostate cancer cells. Cancer Res 2005;65(20): 9185–9. [PubMed: 16230377]
34. Koreckij T, Nguyen H, Brown LG, Yu EY, Vessella RL, Corey E. Dasatinib inhibits the growth of prostate cancer in bone and provides additional protection from osteolysis. Br J Cancer 2009;101(2):263–8. [PubMed: 19603032]
35. Araujo JC, Trudel GC, Saad F, Armstrong AJ, Yu EY, Bellmunt J, et al. Docetaxel and dasatinib or placebo in men with metastatic castration-resistant prostate cancer (READY): a randomised, double-blind phase 3 trial. The Lancet Oncology 2013;14(13):1307–16. [PubMed: 24211163]
36. Schneider M, Korzeniewski N, Merkle K, Schuler J, Grullich C, Hadaschik B, et al. The tyrosine kinase inhibitor nilotinib has antineoplastic activity in prostate cancer cells but up-regulates the ERK survival signal-Implications for targeted therapies. Urol Oncol 2015;33(2):72 e1–7. [PubMed: 24996772]

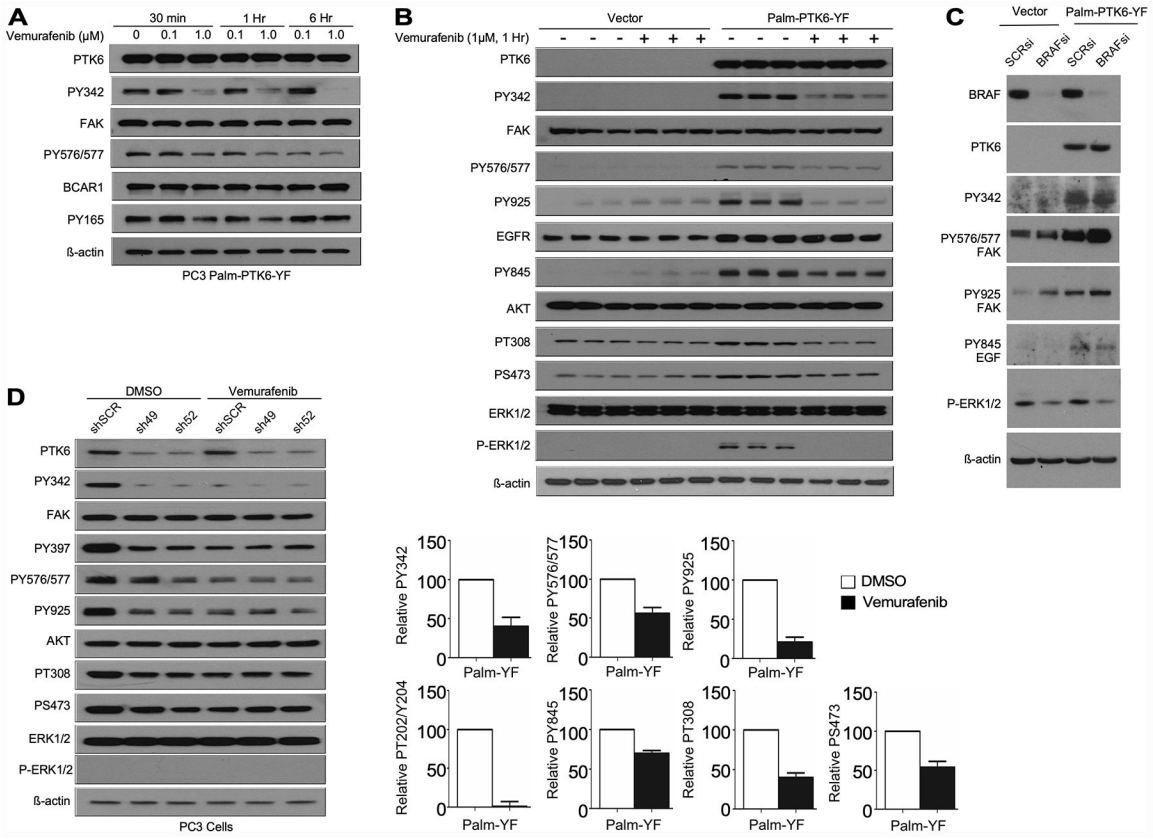

Figure 1. Vemurafenib inhibits activation and signaling downstream of PTK6.

(A) PC3 cells stably expressing Palm-PTK6-YF were treated with vemurafenib or DMSO vehicle and incubated for the times described. Changes in phosphorylation of PTK6, FAK, and BCAR1 were monitored by immunoblotting. Activation of PTK6 is monitored by phosphorylation of Y342. (B) PC3 Vector and PC3 Palm-PTK6-YF cells were treated with vemurafenib and total cell lysates were prepared. Changes in protein levels and phosphorylation were monitored by immunoblotting. Each lane represents one plate of cells (independent experimental replicate). Quantitation of immunoblot data is presented for DMSO and vemurafenib treated Palm-PTK6-YF (Palm-YF) expressing cells in the lower panel. Relative changes in phosphorylation of PTK6 targets were normalized to total protein levels. Residual signal following vemurafenib treatment is displayed ± SEM. (C) siRNA mediated knockdown of BRAF does not inhibit PTK6 activity. Cells were transiently transfected with scrambled or BRAF targeting siRNA (SCRsi and BRAFsi) and harvested at 72 hours. Activating phosphorylation of PTK6 (PY342) and its direct substrates FAK and EGFR are not reduced following knockdown of wild type BRAF. (D) PC3 cells subjected to stable PTK6 knockdown by two shRNA targeting vectors (sh49 and sh52) or scrambled shRNA control (shSCR) were incubated with 1 μM vemurafenib or DMSO vehicle. Similar reductions in downstream signaling are detected in PC3 cells by knockdown of PTK6 (DMSO treated cells) or vemurafenib treatment (shSCR lane). Changes in protein levels and phosphorylation were monitored by immunoblotting.

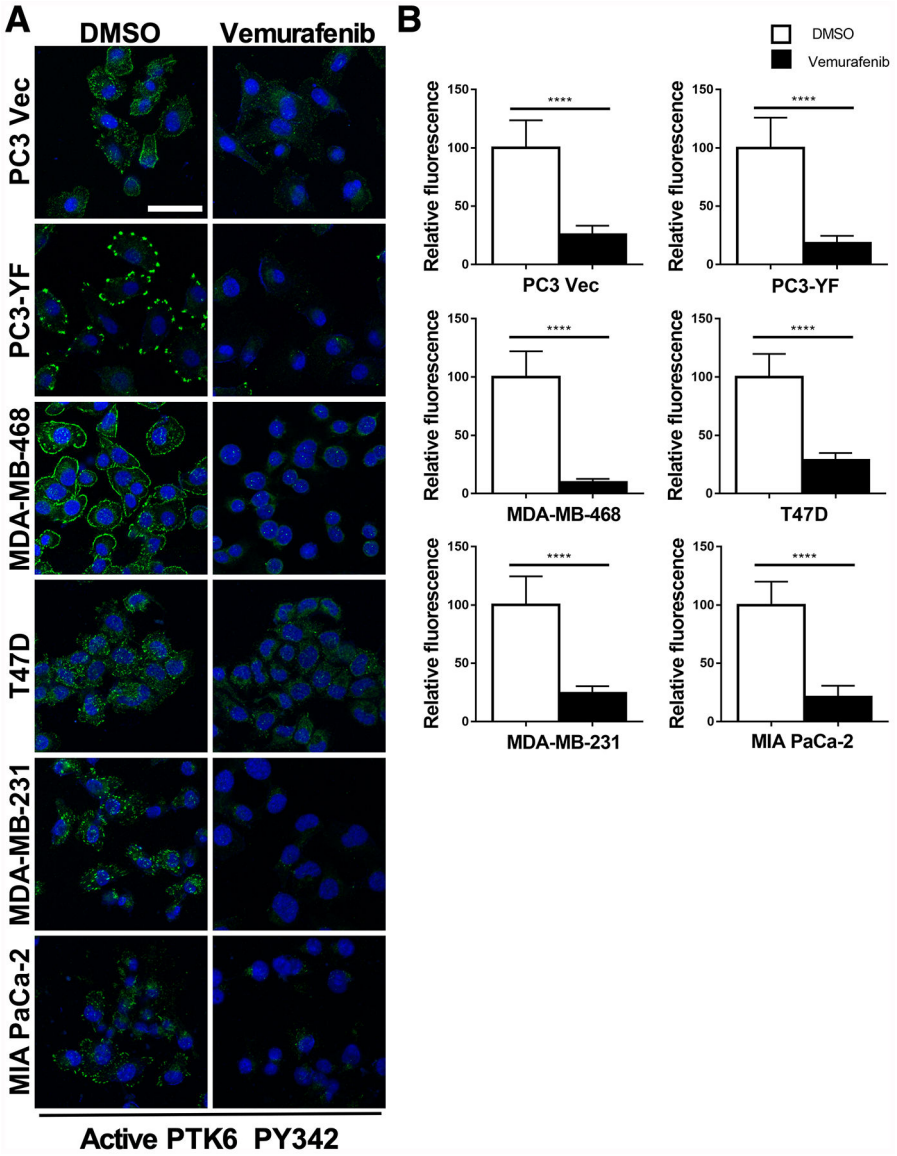

Figure 2. Vemurafenib inhibits PTK6 activation in multiple cell types.

(A) PC3 Vector cells, PC3 cells stably expressing Palm-PTK6 YF (PTK6-YF), MDA-MB-468, T47D, MDA-MB-231 and MIA PaCa-2 cells were treated with DMSO or 1 μM Vemurafenib for 24 hours. Cells were stained for active PTK6 PY342 (Alexa Fluor 488; green). Cells were counterstained with DAPI (blue). Treatment with vemurafenib inhibits active PTK6 in cells of different origin. Scale bar, 50 μm. (B) (B) Quantification of the PY342 Alexa Fluor 488 immunofluorescence signal is presented for the DMSO and vemurafenib treated cells. Signal intensities in vemurafenib treated cells were normalized to the average signal observed in DMSO treated cells and expressed as the average ± SEM. Significance was assessed using the Student's two-tailed *t*-test (n=15 cells/cell type/treatment, **** $P < 0.0001$).

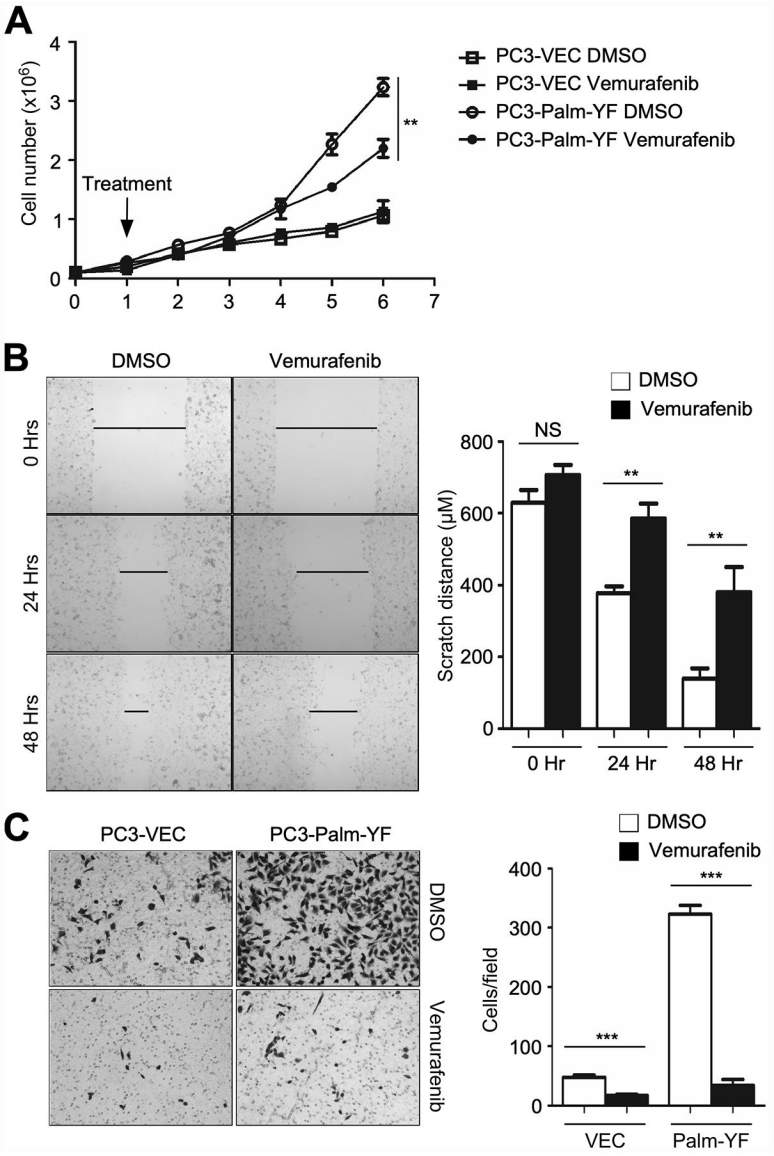

Figure 3. Oncogenic functions of PTK6 are inhibited upon vemurafenib treatment.

(A) PC3 cells expressing empty vector (PC3-VEC) or Palm-PTK6-YF (PC3-Palm-YF) were used in a proliferation assay with the addition of vemurafenib (1μM) or DMSO vehicle. Cell number was plotted ± SEM. Significance was assessed at Day 6 using the Student's two-tailed *t*-test (n=3 independent trials run in triplicate, ** $P < 0.01$). (B) PC3 cells expressing Palm-PTK6-YF were used in a scratch migration assay with the addition of vemurafenib (1μM) or DMSO vehicle. Wound gap distance was measured after the time described ± SEM. Significance was assessed at each time point using the Student's two-tailed *t*-test (n=3 independent trials run in triplicate, ** $P < 0.01$). (C) PC3 cells expressing empty vector or Palm-PTK6-YF were used in a transwell invasion assay with the addition of vemurafenib (1μM) or DMSO vehicle and invaded cells were quantified after 24 hours and plotted ± SEM. Significance was assessed using the Student's two-tailed *t*-test (n=3 independent trials run in triplicate, *** $P < 0.001$).

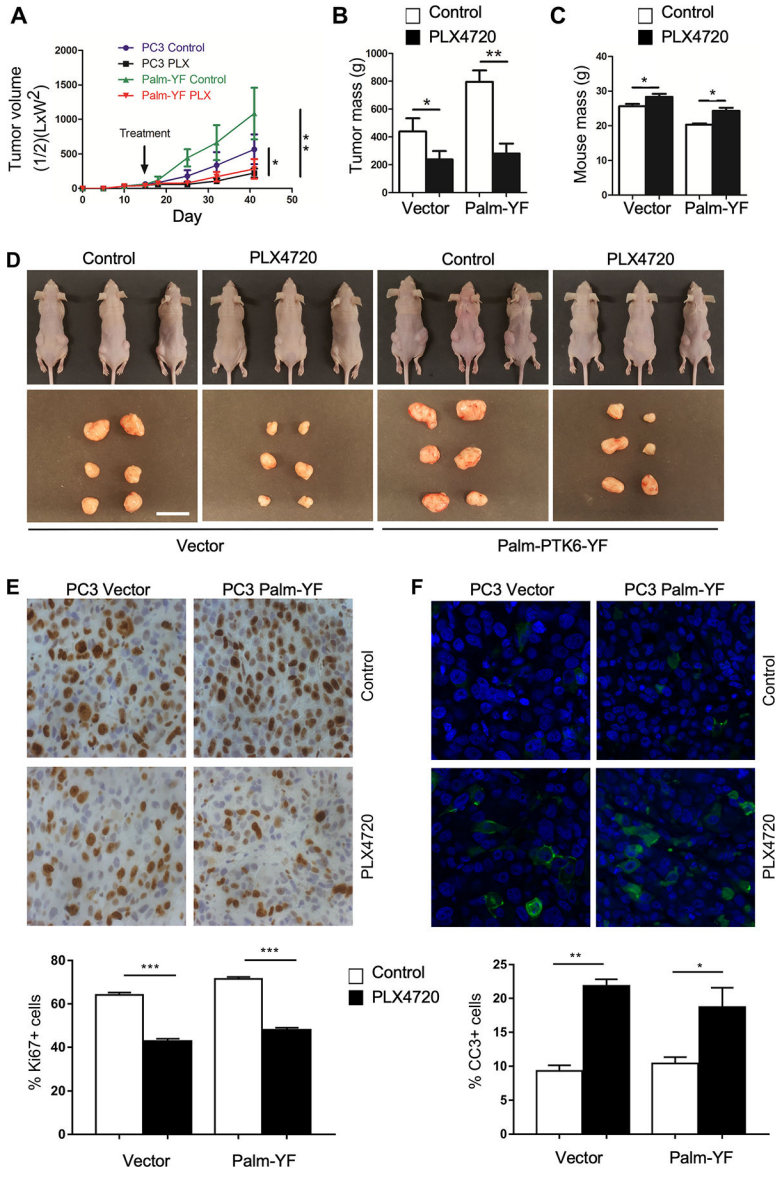

Figure 4. Vemurafenib reduces PTK6-induced tumor burden *in vivo*.

PC3 cells expressing empty vector or Palm-PTK6-YF (PC3-Palm-YF) were injected into the flanks of nude mice. After tumors were palpable (~100 mm^3), the mice were fed control chow or chow containing 417 mg/kg PLX4720 (tool analog of vemurafenib). (A) Tumor volume was measured on a regular basis (n=6/group). Significance was assessed at Day 41 post-injection using the Student's two-tailed *t*-test. (B) At the completion of the study (41 days post-injection), the masses of the tumors were recorded (n=6). Significance was assessed at Day 41 post-injection using the Student's two-tailed *t*-test. (C) At the completion of the study, the masses of the mice were recorded (n=3). Significance was assessed at Day 41 post-injection using the Student's two-tailed *t*-test. (D). At the completion of the study, pictures of the mice and tumors were recorded. Scale bar, 2 cm. (E) Tumors from mice bearing PC3-VEC and PC3-Palm-YF expressing xenografts were sectioned and immunostained for Ki67. (F) Tumors from mice bearing PC3-VEC and PC3-Palm-YF

expressing xenografts were sectioned and immunostained for cleaved caspase-3 (CC3+). For E and F, antibody stained xenograft tumor sections were examined for hot spots, areas of higher staining than the surrounding tissue, and positive cells were counted in at least four different hot spots per tumor sample. Results are expressed as an average ± SEM, and one-way ANOVA followed by Tukey's multiple comparison test (GraphPad Prism 7) were used to determine P-values (bottom panels; n= 5, * $P < 0.05$, *** $P < 0.001$, **** $P < 0.0001$).

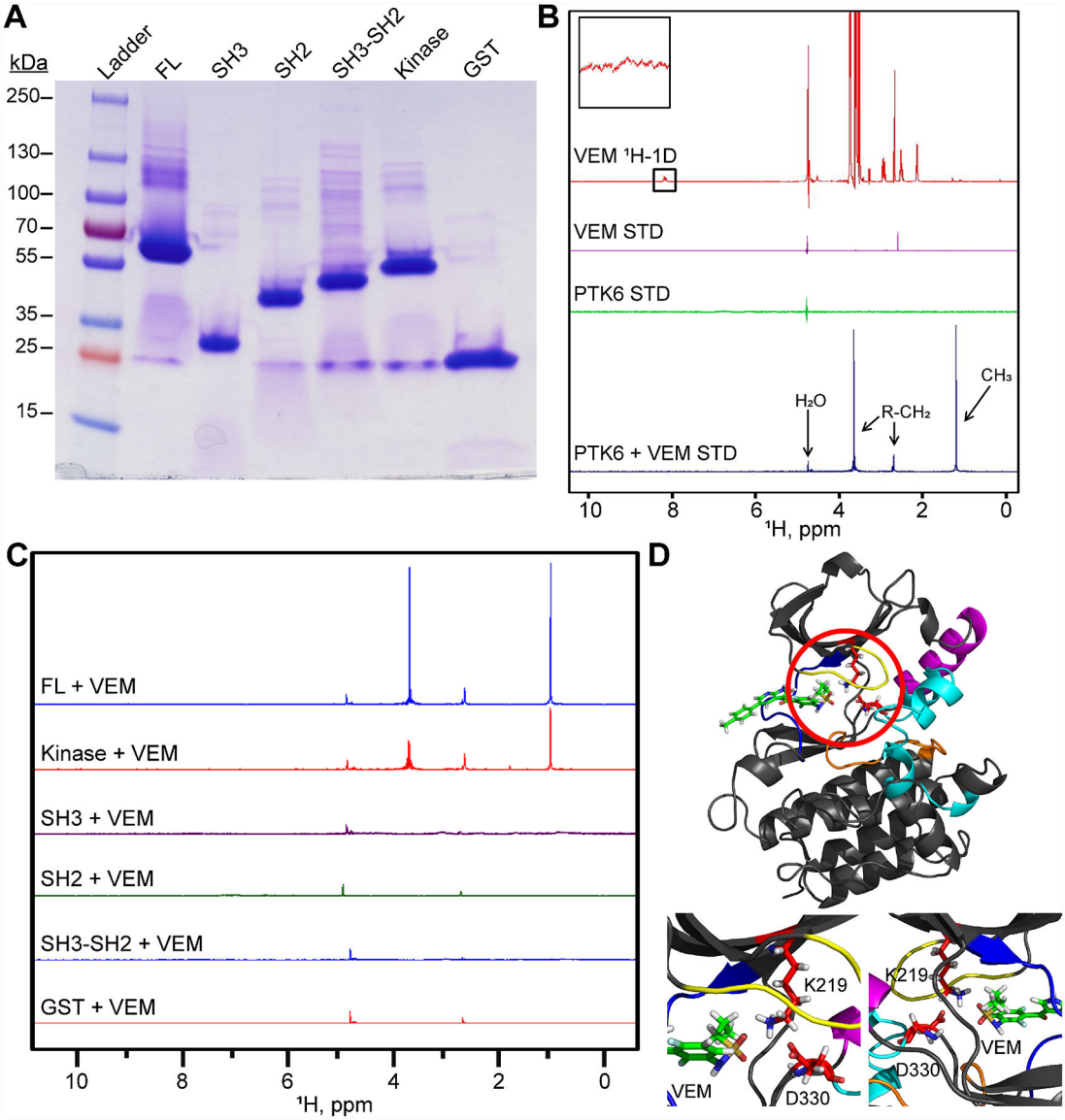

Figure 5. Vemurafenib directly binds the catalytic domain of PTK6.

(A) Full-length (FL), SH3, SH2, SH3-SH2 and kinase domains of PTK6 fused to GST or GST alone were expressed in bacteria and affinity-purified using glutathione agarose. Purified proteins were analyzed by SDS-PAGE. (B) 1D ^{1}H NMR spectrum of 1 mM vemurafenib and STD NMR spectra of vemurafenib (1 mM) alone, GST-FL-PTK6 (10 μM) alone or 1 mM vemurafenib plus 10 μM GST-FL-PTK6. Inset shows signals from 1D ^{1}H NMR spectra of vemurafenib (1 mM) in the aromatic region. (C) STD NMR spectra of GST or PTK6 GST-fusion proteins (10 μM) plus 1 mM vemurafenib. (D) Molecular docking of vemurafenib (green) into the crystal structure of PTK6 (grey) (PMID: 27993680). Distinct regions of the kinase domain are color coded as follows: Pi loop (yellow), α-C helix (magenta), Hinge (blue), HRD loop (orange), DFG loop (cyan), Catalytic triad (red). Magnified images show how the sulfonamide and propyl groups of vemurafenib are oriented towards the PTK6 catalytic triad in our model of the drug-kinase complex.